Journal of Engineering Mathematics (2026) 159:9
https://doi.org/10.1007/s10665-026-10533-3

Optimal operation of floating flywheel energy storage under fluctuating electricity prices

Rory Ward[1] · Graham Benham[2] · Ian Hewitt[3]

Received: 15 January 2026 / Accepted: 21 May 2026

Abstract

Large-scale energy storage is increasingly required to support offshore renewable generation, motivating interest in floating mechanical storage systems. Here we study the large-scale storage of kinetic energy via a floating offshore flywheel. We develop a simple mathematical model for the flywheel dynamics subject to hydrodynamic drag, bounded applied torque, and time-varying electricity prices, with optional wind-driven torque from surface-mounted sails. The operation of the system is formulated as an optimal control problem that maximises net energy revenue over a periodic operating cycle. The resulting optimal control problem is studied using a combination of asymptotic analysis and numerical optimisation. We show that across a wide range of physically relevant parameters, optimal operation reduces to a regime of near-constant angular velocity. In this regime, charging and discharging are governed by a simple switching rule based on a critical electricity price that can be determined directly from price data. Wind-driven torque enhances performance but does not alter the basic switching control structure. Case studies using idealised price profiles and German electricity market data demonstrate how the resulting switching-based control strategy operates under realistic conditions.

Keywords Asymptotic methods · Energy storage systems · Numerical optimisation · Offshore renewable energy · Optimal control

1 Introduction

The rapid expansion of renewable energy sources such as wind and solar has introduced new challenges for electricity systems worldwide. A key issue is intermittency:

✉ Graham Benham
g.benham@ucl.ac.uk

[1] School of Mathematics and Statistics, The University of Melbourne, Parkville, VIC 3010, Australia

[2] Department of Mechanical Engineering, University College London, Gower Street, London WC1E 6BT, UK

[3] Mathematical Institute, University of Oxford, Oxford OX2 6GG, UK

Published online: 16 July 2026

supply fluctuates with weather conditions, while demand can change sharply and unpredictably [1, 2]. To ensure reliable operation, future low-carbon grids will require a substantial increase in large-scale energy storage capacity. For example, to meet net-zero targets in the UK, the required storage capacity must rise from around 5 GW today to more than 50 GW by 2050 [3, 4]. Developing technologies that can provide cost-effective, large-scale storage is therefore a critical research priority [5].

Existing storage solutions each have strengths and limitations. Pumped hydropower (such as the Dinorwig power station in Wales [6]) offers high capacity but is geographically restricted. Electrochemical batteries are flexible but face challenges of degradation [7], safety (e.g. fire and explosions) [8, 9], and environmental impact [5, 10]. Other concepts such as compressed air storage [11], thermal energy storage [12, 13], and hydrogen electrolysis [14] continue to be developed but have yet to achieve widespread deployment. This motivates exploration of alternative storage technologies that may complement existing options.

Another possible solution may be found in the large-scale storage of kinetic energy via an offshore flywheel. One such example called *Gyrerg* has been developed by *VerdErg Renewable Energy Limited* in the UK [15]. This takes the form of a large concrete flywheel that floats on the water surface (via a pressurised air cushion), and stores energy mechanically by rotating (see Fig. 1b). Large scales are required to store significant quantities of energy,—for example, a 900 m radius flywheel can store 1 GWh of energy if rotating at one revolution per 8.5 min (See Appendix A). Flotation is achieved by introducing a void space beneath the annulus, whereby the weight of the concrete is balanced by a pressurised air cushion beneath. This enables supporting potentially millions of tonnes of concrete while also reducing the wetted surface area and hence the hydrodynamic drag from the sea. To accelerate or decelerate the flywheel, a torque is applied via wheels (or other means) positioned at the circumference. The ability to float the flywheel enables placement near offshore wind farms to store excess energy generated from wind turbines. Since the drag forces on the wetted surfaces (and therefore energy losses) are significant, any potential methods for offsetting this lost energy would increase the viability of such a technology. One such idea is to place a number of large sails on the upper surface to provide ‘free’ wind energy to offset these losses (see Fig. 1c).

Previous flywheel studies have primarily focused on land-based systems to stabilise the grid [16, 17] and to generate revenue via trading [18]. Some studies, such as [19], have investigated the use of a flywheel to regulate energy from offshore renewables (e.g. wind farms and marine-current farms). However, no optimisation framework has been developed for floating flywheels, for which acceleration is crucially in opposition to hydrodynamic drag from the water. Moreover, floating flywheels have the additional feature of being able to extract energy directly from the wind via sails, thereby acting as a hybrid between a flywheel and a conventional wind turbine. None of these features specific for floating flywheels (hydrodynamic drag, wind-assisted operation) have been modelled or optimised before, which restricts their use for grid stabilisation or revenue generation in a fluctuating electricity market.

This work develops the first mathematical framework for optimal control of a floating flywheel energy storage system under dynamic electricity prices. The framework integrates hydrodynamic drag losses and optional sail-driven torque within an ana-

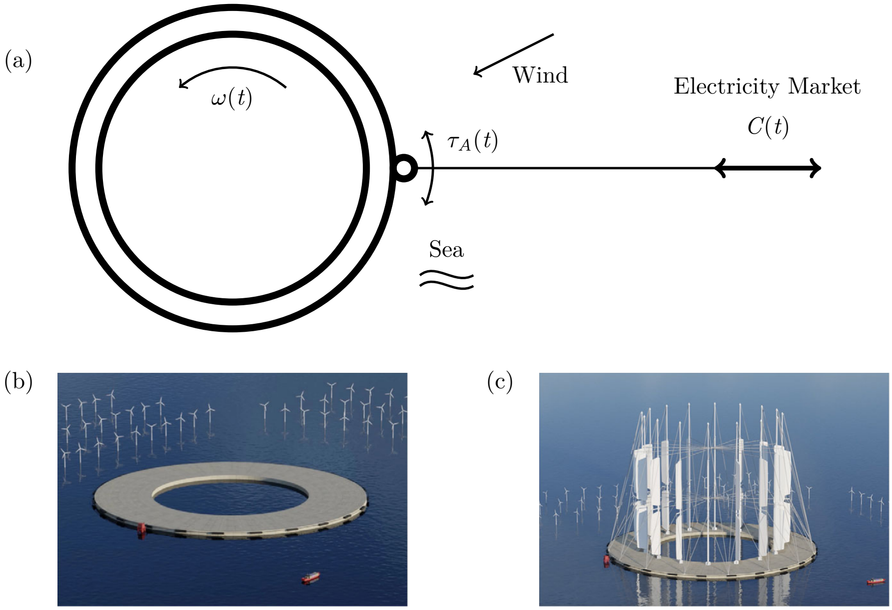

Fig. 1 **a** Schematic diagram (plan view) depicting a large floating flywheel accelerated/decelerated by an applied torque $\tau_A(t)$, with additional torques due to the wind and due to friction from the sea. Electricity is either bought from (to accelerate the flywheel) or sold to (to decelerate it) the electricity market at some price $C(t)$. **b** *VerdErg*'s conceptual design of *Gyrerg*, illustrating the ability to store energy from neighbouring offshore wind farms. **c** Conceptual design with sails on top. Both **b** and **c** are taken with permission from [15]

lytical and numerical optimisation scheme. We formulate an optimal control problem in which the applied torque serves as the decision variable and the net revenue is the performance objective. Three price scenarios are considered: (i) step-change fluctuations, (ii) sinusoidal variations, and (iii) real electricity market data from Germany. Analytical and numerical methods reveal a range of operational behaviours, including bang-bang and singular control regimes. Importantly, under realistic parameter values, the system operates in a simple regime where the flywheel spins at nearly constant velocity and charging/discharging decisions reduce to switching around a critical price threshold. This result provides a practical, low-complexity control strategy requiring minimal forecasting.

Finally, we investigate the role of wind-driven sails in enhancing performance by generating additional revenue even when electricity prices are constant. The framework we develop provides both fundamental insights into the control of flywheel storage technologies as well as practical guidance for their potential integration into future energy systems.

2 Problem formulation

We consider the control of a large annular flywheel floating on the surface of the sea, as depicted in Fig. 1a. A torque $\tau_A(t)$ is applied to the flywheel which spins at angular velocity $\omega(t)$ around a fixed vertical axis at its centre. The applied torque may either be positive, whereby electricity is bought from the grid at price $C(t)$ and used to turn the flywheel, or negative, whereby power is drawn from the flywheel to decelerate it and electricity is sold back to the grid at price $C(t)$ (buy and sell rates are assumed to be the same for simplicity). The rotating device undergoes friction by contact with the surrounding water, resulting in a drag torque τ_D. As an optional feature of the setup, we may also consider sails attached to the upper surface of the flywheel, such that an additional torque τ_S may be generated by the wind.

A simple model for the dynamics of the system is the following conservation of momentum equation

$$I\frac{\mathrm{d}\omega}{\mathrm{d}t} = \tau_A + \tau_S - \tau_D, \tag{1}$$

where I is the moment of inertia of the flywheel. In addition, we use the following quadratic inertial law for the drag due to the seawater in the limit of large Reynolds number,

$$\tau_D = I_D\omega^2, \tag{2}$$

where I_D is a drag-related constant with the same dimensions as the moment of inertia. There are a variety of complexities in modelling I_D, including turbulent and viscous friction, boundary layer separation, and effects due to the acceleration/deceleration of the surrounding seawater. However, in the first instance, we choose to neglect such details and simply treat I_D as a constant. Later in Appendix A, we discuss this drag law in more detail, including an estimate of the order of magnitude of I_D based on a scaling law for high Reynolds number turbulent flows. The torque due to the optional sails τ_S is modelled in more detail in Sect. 3.

We assume that the cost of electricity per unit of energy $C(t)$ is periodic in time with period T_0 (e.g. 1 week or 1 year) and we denote the revenue made as R. We also assume that electricity can be bought and sold without restriction when needed. That is, the applied torque is only limited by engineering constraints, as opposed to lack of supply or demand to the grid. In particular, we consider linear constraints applied to the torque of the form

$$-\tau_{\max} \leq \tau_A(t) \leq \tau_{\max}, \tag{3}$$

where $\tau_{\max}$ is the maximum possible torque that can be used to charge/discharge the system. We note that another variation of this problem uses the applied power $P_A(t) = \tau_A(t)\omega(t)$ as the control variable, with equivalent bounds on the maximum power used to charge/discharge the system. However, we do not go into the details here since the methodology is similar.

The revenue per unit time is given by the product of the negative electricity price per unit energy, $-C(t)$, and the applied power, $P_A(t) = \tau_A(t)\omega(t)$. Hence, the total revenue generated over the time interval $[0, T_0]$ is given by

$$R\left[\tau_A(t)\right] = \int_0^{T_0} -C(t)\tau_A(t)\omega(t)\,\mathrm{d}t. \tag{4}$$

With the goal of increasing revenue, we therefore seek to maximise R over the period of operation, where R is a functional of the applied torque.

Since the cost function $C(t)$ is periodic with period T_0, so too must be the dynamics of the system. As such, we accompany (1) with the following periodic boundary condition

$$\omega(0) = \omega(T_0). \tag{5}$$

Finally, for the sake of consistency and to avoid confusion between negative/positive applied torques and angular velocities, we restrict our attention to nonnegative angular velocities only. Hence, we impose the additional constraint (accompanying (1)) that

$$\omega(t) \geq 0. \tag{6}$$

We nondimensionalise the system using the scalings

$$\begin{aligned} &\omega \sim \left(\frac{\tau_{\max}}{I_D}\right)^{1/2}, \quad \tau_A, \tau_S \sim \tau_{\max}, \quad t \sim \frac{I}{(I_D\tau_{\max})^{1/2}}, \\ &C \sim C_{\max}, \quad R \sim \frac{I\tau_{\max}C_{\max}}{I_D}, \end{aligned} \tag{7}$$

where $C_{\max}$ is the maximum price over the period of operation. These scalings result in the nondimensionalised system

$$R\left[\tau_A(t)\right] = \int_0^{T} -C(t)\tau_A(t)\omega(t)\,\mathrm{d}t, \tag{8}$$

$$-1 \leq \tau_A(t) \leq 1, \tag{9}$$

$$\frac{\mathrm{d}\omega}{\mathrm{d}t} = \tau_A(t) + \tau_S(t) - \omega(t)^2, \tag{10}$$

$$\omega(t) \geq 0, \tag{11}$$

$$\omega(0) = \omega(T), \tag{12}$$

where the dimensionless period is given by

$$T = \frac{T_0(I_D\tau_{\max})^{1/2}}{I}. \tag{13}$$

In summary, our objective is to maximise (8) by varying the control $\tau_A(t)$ subject to the linear constraint (9) and the constraint that (10)–(12) are satisfied.

2.1 Electricity price

We have chosen three possible price functions to represent behaviour in electricity prices, as shown in Fig. 2. The first of these is simply a step-change in price that alternates between a minimum $C_{\min}$ and a maximum $C_{\max}$. In dimensionless terms, this is given by

$$C(t) = \begin{cases} 1, & 0 \le t < \frac{T}{2}, \\ C_0, & \frac{T}{2} \le t < T, \end{cases} \tag{14}$$

where $C_0 = C_{\min}/C_{\max} \in [0, 1]$. This periodic two-level price function represents dramatic changes in electricity price, e.g. due to weather or large-scale events.

The second price function that we investigate is of a sinusoidal form. This could represent smoother daily fluctuations, or longer term seasonal fluctuations. In this case, the dimensionless price is given by

$$C(t) = \frac{1 + C_0}{2} + \frac{1 - C_0}{2} \cos\left(\frac{2\pi t}{T}\right). \tag{15}$$

The third price function is based on average German electricity price over the course of a week (data taken from 2015 to 2021), as shown in Fig. 2c. This *European Wholesale Electricity Price Data* is provided by *Ember Energy* and the time period (2015–2021) is chosen because these are the data that are freely available from [20]. The original dataset consists of hourly electricity prices over the period 2015–2021. To obtain a representative periodic price over the course of one week, we partition the data into weekly intervals and average each hour-of-week across all weeks in the dataset. More precisely, if C_n denotes the hourly electricity price from the dataset and $t \in [0, 167]$ denotes the hour within a week, then the representative weekly profile is constructed as

$$C(t) = \frac{1}{W} \sum_{k=0}^{W-1} C_{168k+t}, \tag{16}$$

where $W = 536$ is the number of complete weeks. This procedure preserves the characteristic weekday/weekend structure of the market while filtering irregular week-to-week fluctuations and external events specific to individual time periods. The resulting price profile therefore represents a typical weekly variation rather than any specific historical week.

Over the course of this representative week, the price fluctuates between around 29 EUR and 111 EUR per MWh of electricity, resulting in a dimensionless value of $C_0 = 0.26$. Each day of the week has two distinct peaks in price (corresponding roughly to before and after the working day) and there is a characteristic drop in price on the weekend.

2.2 Solving the optimal control problem in the absence of wind

To begin with we will study the case where there are no sails (or simply no wind), for which the torque term $\tau_S = 0$. Using the theory of optimal control [21], the

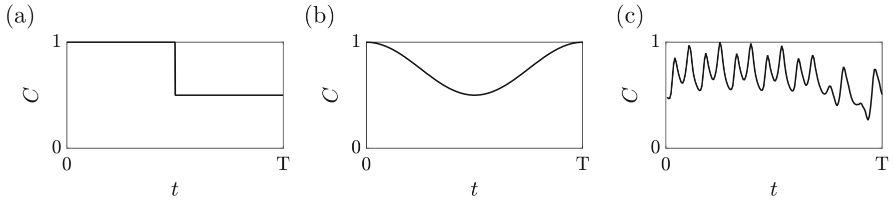

Fig. 2 Electricity price functions given in dimensionless terms. **a** Periodic step-change price (14). **b** Sinusoidal price (15). **c** Average German electricity price over the course of a week (2015–2021), taken from [20]

Hamiltonian (the objective plus a Lagrange multiplier times the ODE constraint) is given by

$$H = -C(t)\omega(t)\tau_A(t) + \lambda(t)\left(\tau_A(t) - \omega(t)^2\right), \tag{17}$$

where we are considering the applied torque $\tau_A(t)$ as the control variable and $\lambda(t)$ is the adjoint variable. The optimal solution for the applied torque minimises the Hamiltonian, but since (17) is linear in τ_A this is either achieved at the bounds $\tau_A = \pm 1$ or on a 'singular arc'. If the control variable is always at its limiting bounds, this is referred to as 'bang-bang', whereas if it lies between its limiting bounds for a non-zero time interval, this is referred to as a singular arc.

To determine the form of singular arcs we substitute $\tau_A(t)$ from (10) into (8), and perform a calculus of variations to the angular velocity $\omega(t)$. The revenue is then rewritten as

$$R\left[\omega(t)\right] = \int_0^T -C(t)\omega(t)\left(\dot{\omega}(t) + \omega(t)^2\right)\mathrm{d}t. \tag{18}$$

The Euler–Lagrange equation for (18) requires that singular arcs (if present) take the form

$$\omega^*(t) = 0 \quad \text{or} \quad \omega^*(t) = \frac{\dot{C}(t)}{3C(t)}, \tag{19}$$

where asterisks indicate an optimum. Hence, singular arcs are either given by a stationary system or by relating the angular velocity to the logarithmic derivative of the price function. Since the angular velocity and the price are both nonnegative, the non-zero singular arc (19) can only exist if the electricity prices are increasing $\dot{C} > 0$. The corresponding applied torque is given by

$$\tau_A^*(t) = 0 \quad \text{or} \quad \tau_A^*(t) = \frac{1}{9C(t)^2}\left(3C(t)\ddot{C}(t) - 2\dot{C}(t)^2\right). \tag{20}$$

We note that bang-bang control, while not necessarily always optimal, may be the easiest operation strategy to implement. In contrast, the singular arcs may require more accurate price forecasts as well as more precise control. An extension of this work could involve stochastic control, whereby uncertainty in the future electricity price is accounted for in the optimisation [22, 23].

As an alternative to the above Euler–Lagrange approach, we may also calculate optimal solutions numerically. These solutions are determined by discretising (10) in time, and then solving for the discrete values of angular velocity and applied torque that satisfy (9)–(12), and which maximise the revenue (8). The code is run with the *JuMP* package of the *Julia* programming language [24] using the *Ipopt* solver [25], which is an implementation of the interior-point method. All simulations were run with a relative convergence tolerance of 10^{-8} and a maximum of 2000 iterations, which was sufficient to ensure convergence of both the objective function and dynamics. Convergence was verified by repeating selected simulations with progressively refined time discretisations, confirming that the optimal revenue and switching behaviour were insensitive to further refinement. For reproducibility, the key model parameters, solver settings, and a fully annotated example implementation (including code version and package dependencies) are publicly available in the accompanying repository (see Sect. 5 for availability statement).

Next, each of the above price functions are investigated using numerical optimisation and verified using analytical results where possible.

2.3 Step-change price fluctuations

For a step-change price function (14), there will be no non-zero singular arcs (19) since these relate to derivatives of the price function. Hence, the stationary singular arc is the only possible singular behaviour in this case. There are only 2 dimensionless parameters that define the problem, which are $C_0 \in [0, 1]$ and $T > 0$. A variety of optimal solutions acquired via numerical optimisation are displayed in Fig. 3b–e, for different values of C_0 and T. There are two types of control: Bang-Bang BB (where the control is only ever at its limits) and Bang-Singular BS (where there are stationary intervals). Two BB solutions are shown in Fig. 3c, e, for different values of C_0 and T, and two BS solutions are shown in Fig. 3b, d. The solution behaviour involves discharging (when electricity is expensive) before charging (when electricity is cheap), with a possible stationary period in between. A curve in Fig. 3a delineates between the cases of BB and BS, which is derived analytically below.

Motivated by our numerical solution, we next follow an analytical approach where we posit the behaviour of the optimal control as follows:

$$\tau_A(t) = \begin{cases} -1, & 0 < t < t_1, \\ 0, & t_1 < t < t_2, \\ 1, & t_2 < t < T, \end{cases} \tag{21}$$

where t_1 and t_2 are the switching times for discharging, being stationary (if relevant), and charging. The corresponding analytical solution to (10) for the angular velocity is

$$\omega(t) = \begin{cases} \tan\left(\arctan\left(\omega_0\right) - t\right), & 0 < t < t_1, \\ 0, & t_1 < t < t_2, \\ \tan h(t - T + \operatorname{arctan} h(\omega_0)), & t_2 < t < T, \end{cases} \tag{22}$$

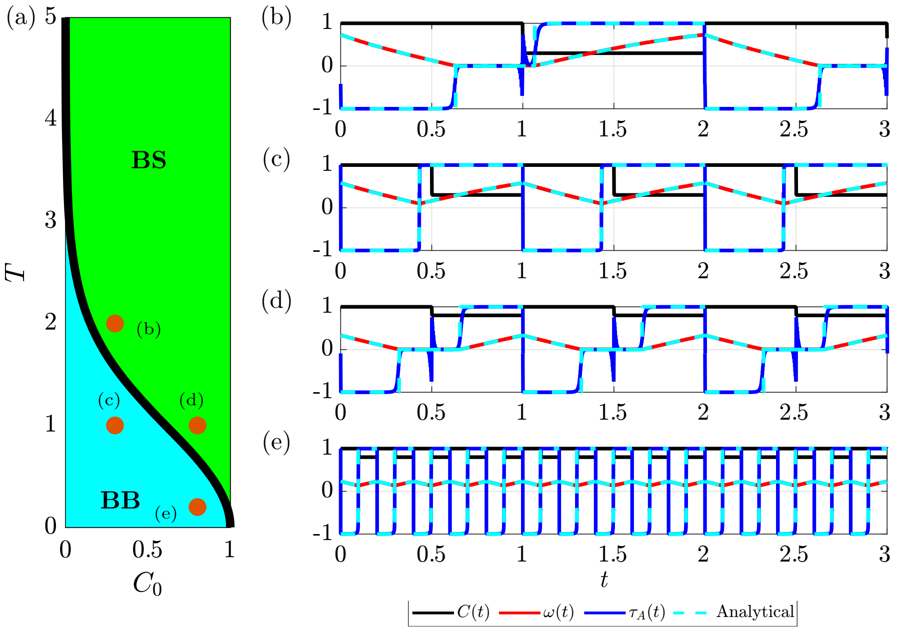

Fig. 3 Optimal control strategies for a step-change price. Colours in **a** indicate Bang-Bang (BB) and Bang-Singular (BS) control. Different example strategies are displayed in **b**–**e** for different values of C_0 and T. (Color figure online)

where $\omega_0 = \omega(0)$ is the maximum angular velocity at the initial time.[1]

In order for there to be some stationary period, we require that $t_1 < t_2$. Since, in this scenario, the angular velocity is zero at both t_1 and t_2, we can determine that

$$t_1 = \arctan(\omega_0), \quad t_2 = T - \operatorname{arctan}h(\omega_0), \tag{23}$$

and hence there will be some stationary period if

$$T > \arctan(\omega_0) + \operatorname{arctan}h(\omega_0). \tag{24}$$

For situations which satisfy (24) the device ought to be stationary for some interval according to (22). In this case, the revenue earned over one period can be determined as

$$R = \int_0^{t_1} C(t)\tan(t_1 - t)\mathrm{d}t - \int_{t_2}^{T} C(t)\tan h(t - t_2)\mathrm{d}t, \tag{25}$$

[1] Note, it is possible to include an additional parameter t_0 for the phase difference between $t = 0$ and the maximum value of ω. However, it is straightforward to show that the optimum t_0 is 0, such that the maximum value of ω occurs at $t = 0$.

where ω_0 is chosen to maximise the revenue. For the case where the price drop happens during the stationary period $t_1 < T/2 < t_2$ (such that $C = 1$ and $C = C_0$ in the first and second integrals above), we get

$$\frac{\partial R}{\partial \omega_0} = \frac{\omega_0}{1+\omega_0^2} - \frac{C_0 \omega_0}{1-\omega_0^2}. \tag{26}$$

Here, R is minimised at $\omega_0 = 0$ and maximised at

$$\omega_0 = \sqrt{\frac{1-C_0}{1+C_0}}. \tag{27}$$

We can also see that for $C_0 \in (0, 1)$, we have $\omega_0 \in (0, 1)$. The total revenue given by this maximum is

$$R = \frac{1+C_0}{2} \log\left(\frac{2}{1+C_0}\right) + \frac{C_0}{2} \log C_0. \tag{28}$$

This is a monotone decreasing function of C_0, with $R = 0$ when $C_0 = 1$ (no price change) and $R = \frac{1}{2}\log(2)$ when $C_0 = 0$ (maximum price change). The optimum value (27) can be inserted into (24) to give the following condition required for a stationary singular arc to exist

$$T > \arctan\left(\sqrt{\frac{1-C_0}{1+C_0}}\right) + \arctan h\left(\sqrt{\frac{1-C_0}{1+C_0}}\right). \tag{29}$$

This curve is plotted in Fig. 3a, showing the division between BB and BS solutions.

If, instead (29) is not satisfied, then the device will never become stationary in the time period $[0, T]$ and we have the angular velocity given by

$$\omega(t) = \begin{cases} \tan\left(\arctan\left(\omega_0\right) - t\right), & 0 < t < t_s, \\ \tan h(t - T + \arctan h(\omega_0)), & t_s < t < T, \end{cases} \tag{30}$$

where t_s is the time when operation switches from discharging to charging. If we denote $\omega(t_s) = \omega_s$ and use the fact that the angular velocity must be continuous at t_s, then we have two equations relating the angular velocity to the time at the switching point,

$$\omega_s = \tan\left(\arctan\left(\omega_0\right) - t_s\right), \tag{31}$$

$$\omega_s = \tan h(t_s - T + \arctan h(\omega_0)), \tag{32}$$

which can be solved simultaneously for t_s and ω_s, given ω_0 and T. In this case, the revenue is given by

$$
\begin{aligned}
R = &\int_0^{t_s} C(t) \tan\left(\arctan\left(\omega_0\right) - t\right)\, \mathrm{d}t \\
&- \int_{t_s}^{T} C(t) \tan h(t - T + \operatorname{arctan}h(\omega_0))\, \mathrm{d}t.
\end{aligned}
\tag{33}
$$

As before, finding the optimum value of ω_0 requires setting $\partial R/\partial\omega_0 = 0$. However, since t_s and w_s are related implicitly through (31) and (32), we cannot determine an analytical expression for the optimum ω_0 in this case. Nevertheless, the form of the solution has been determined and can be validated against numerically optimised solutions.

We compare numerical and analytical solutions in Fig. 3b–e, for different values of C_0 and T. Close comparison is observed except for some numerical oscillations near the discontinuous price switch that are hard to eliminate[2]. We also show the optimal revenue as a contour plot of C_0 and T in Fig. 5a. We see that more revenue is achieved for long periods and large price jumps, which makes sense intuitively.

It is interesting to note that for very small periods $T \ll 1$, the angular velocity remains almost constant such that $\omega \approx \omega_0$, for all time, as shown in Fig. 3e (where $C_0 = 0.8$ and $T = 0.2$). Therefore, what appears to be a singular arc is in fact the result of very rapid bang-bang control maintaining a constant ω value. Asymptotic analysis of (31)–(33) in this limit reveals that to leading order, the switching time and revenue are

$$t_s \approx \frac{T}{2}(1 - \omega_0^2), \tag{34}$$

$$R \approx \frac{1}{2} T\omega_0(1 - C_0 - 2\omega_0^2). \tag{35}$$

Hence, the non-zero value of ω_0 that maximises revenue ($\partial R/\partial\omega_0 = 0$) is

$$\omega_0 \approx \sqrt{\frac{1 - C_0}{6}}. \tag{36}$$

The above approximation shows good agreement with numerically optimised solutions for small T values. For example, Fig. 3e shows angular velocities in the range $\omega \in [0.13, 0.23]$, compared to $\omega_0 = 0.183$ as calculated using (36) with $C_0 = 0.8$ and $T = 0.2$ (note, the approximation gets better as T gets smaller). It is also worth noting that the mean torque in this approximation is given by

$$\bar{\tau}_A \approx \omega_0^2 \approx \frac{1 - C_0}{6}, \tag{37}$$

[2] We have tried increasing the number of grid points as well as forward, backward and central finite difference schemes, but the oscillations near the price jump persisted in all cases. Since BB and BS are the only possibilities for this case, the oscillations must be a numerical artefact and should therefore be ignored.

which can be seen by integrating (10) over one period. By substituting (36) into (35) we can write the optimised revenue as

$$R \approx \frac{1}{3} T \omega_0 (1 - C_0) \geq 0, \tag{38}$$

and hence a positive revenue can always be made for small periods $T \ll 1$.

2.4 Sinusoidal price fluctuations

In the case where the price varies sinusoidally (15), non-zero singular arcs (19) are permitted whenever $\dot{C} > 0$ (i.e. for $T/2 < t < T$). As with the above example, here the only dimensionless parameters in the problem are C_0 and T. Numerically optimised solutions are plotted in Fig. 4b–e, for different values of C_0, T. Unlike the previous case, here there is a new possible type of solution in which the optimal control is purely Singular (S) (including both stationary and non-stationary singular arcs). Also, unlike the previous case, the lines delineating regions of solution space (BB/BS/S) are not available analytically, so are approximated using the numerical solutions instead. For small C_0, T, bang-bang control is optimal since singular values of τ_A^* (20) lie beyond the constraints due to large derivatives in price. For large C_0, T, price derivatives and consequently non-zero singular arc values τ_A^* (20) are small enough to be permissible. It is also worth noting that the numerical oscillations observed in the previous case are no longer present here due to the lack of discontinuous price jumps.

The optimal revenue generated for different values of C_0 and T is shown as a contour plot in Fig. 5b. Unlike the step-change price, here we see that for a given value of C_0 there is an optimum value of T that is finite (dashed black line). It is also interesting to note that the overall revenue generated is less for the sinusoidal price than the step-change price, indicating that sharper changes in price are more profitable.

Further analytical progress is possible in the limit of small price fluctuations $C_0 \approx 1$. To study this, we let $C_0 = 1 - \epsilon$, where $\epsilon \ll 1$ is a small parameter. Then, the optimal solution is approximated as

$$\omega(t) \approx \begin{cases} 0 : & 0 < t < T/2, \\ -\frac{\pi}{3T} \sin\left(\frac{2\pi t}{T}\right)\epsilon : & T/2 < t < T, \end{cases} \tag{39}$$

$$\tau_A(t) \approx \begin{cases} 0 : & 0 < t < T/2, \\ -\frac{2\pi^2}{3T^2} \cos\left(\frac{2\pi t}{T}\right)\epsilon : & T/2 < t < T, \end{cases} \tag{40}$$

where we enforce that the angular velocity must be zero when $\dot{C}(t) < 0$. Analytical approximations for ω and τ_A (39) and (40) are compared with numerically optimised solutions in Fig. 4d, for which $T = 1.5$ and $C_0 = 0.9$ (or correspondingly, for $\epsilon = 0.1$). Overall, broad agreement is observed but the numerically optimised solution is overly smoothed at the discontinuous jumps in τ_A.

The other limit of interest is when the period is very short $T \ll 1$, as shown in Fig. 4e (for which $C_0 = 0.3$ and $T = 0.2$). In this case, the angular velocity remains almost constant such that $\omega \approx \omega_0$, similarly to the case of the step-change price.

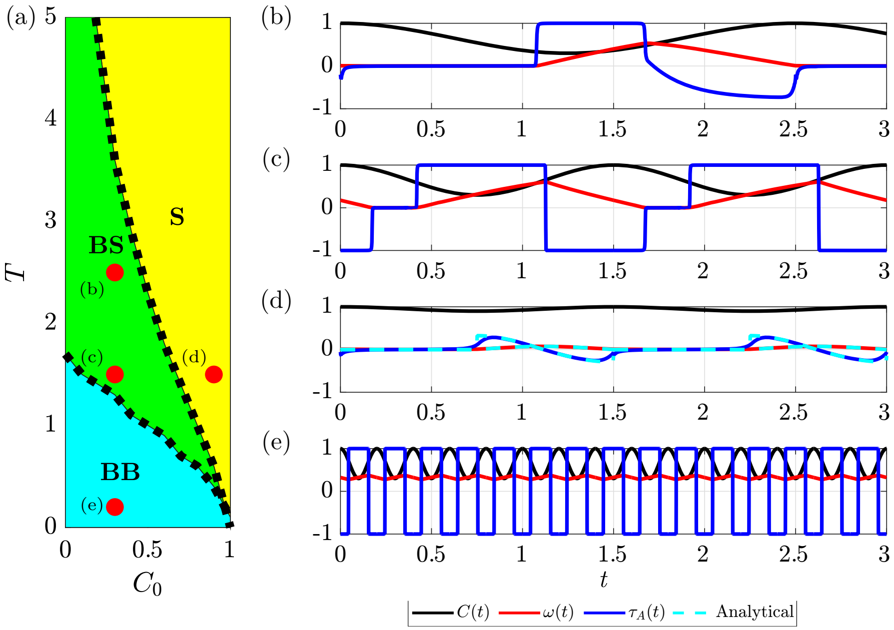

Fig. 4 Optimal control strategies for a sinusoidal price. Colours in **a** indicate Bang-Bang (BB), Bang-Singular (BS) and Singular (S) control. Different example strategies are displayed in **b**–**e** for different values of C_0 and T. Analytical/approximate solutions are only displayed where available. (Color figure online)

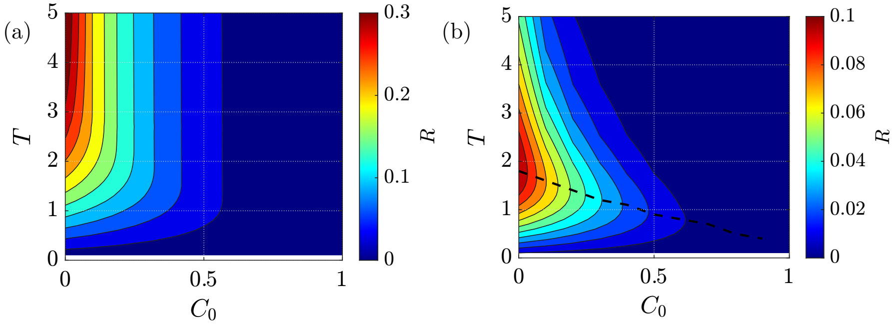

Fig. 5 Revenue in the case of **a** step-change price and **b** sinusoidal price. A dashed black line in **b** indicates the maximum revenue for a given cost ratio C_0, and therefore the optimum period of operation T

We could proceed with asymptotic analysis to find an approximate value of ω_0, as we did before. Instead, we demonstrate a more practical method based on the statistics of the price function. In particular, by looking more closely at the switching dynamics, we notice that switching occurs every time the price increases above a critical value, which we denote C_c. This is illustrated in Fig. 6a for a very small period $T = 0.01$. We have highlighted the price at the switching moments and observe that they all occur at a critical cost of $C_c = 0.71$. This critical cost can be interpreted as the price

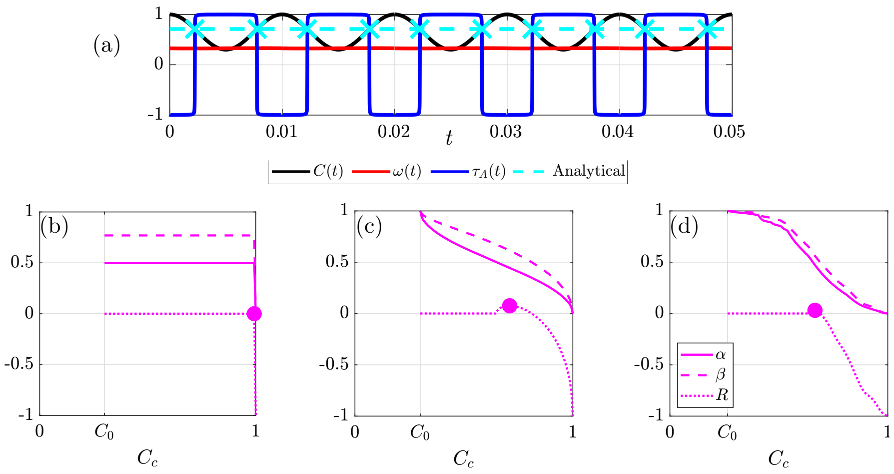

Fig. 6 **a** Optimal control strategy for a sinusoidal price with $C_0 = 0.3$ and a very small period $T = 0.01$, showing that switching occurs at a critical cost of $C_c = 0.71$. **b**–**d** Relative amount of time α and price β above the critical cost C_c (44) and (45), showing where revenue (46) is maximised with a marker, for each of the three different price functions: **b** Step-change, **c** Sinusoidal, **d** German data. Revenue is set to $R = 0$ for $\alpha < 1/2$ to maintain real values

below which it is worth charging the device and above which it is not. Similar such problems (where bang-bang control switches around a critical cost) frequently arise in economics and other problems involving the optimisation of finite resources [21, 26].

Following from this observation, we posit that the optimal control for small periods can be approximated as

$$\tau_A(t) = \begin{cases} -1: & C(t) > C_c, \\ 1: & C(t) < C_c. \end{cases} \tag{41}$$

It is possible to prove (following the approach of [27]) that the optimal control is in fact bang-bang around a critical cost, but we do not go into the details here. Instead, we move forward with the above ansatz and we note by inserting (41) into the formula for the revenue (8), we can write

$$R = \omega_0 \int_{I_1} C(t)\,\mathrm{d}t - \omega_0 \int_{I_2} C(t)\,\mathrm{d}t, \tag{42}$$

where $I_1 = \{t : C(t) > C_c\}$ and $I_2 = \{t : C(t) < C_c\}$ are the time intervals above and below the critical cost. Likewise, the near-constant angular velocity is decomposed as

$$\omega_0 \approx \left(\frac{1}{T}\int_0^T \tau_A(t)\,\mathrm{d}t\right)^{1/2} = \frac{1}{T^{1/2}}\left(-\int_{I_1}\mathrm{d}t + \int_{I_2}\mathrm{d}t\right)^{1/2}. \tag{43}$$

From the above, we see that we must have $\bar{\tau}_A \geq 0$, which implies that $I_1 \leq T/2$. In other words, no more than half the total time must be spent above the critical cost. The relative amount of time and price above the critical cost are defined, respectively, as

$$\alpha(C_c) = \frac{1}{T}\int_{I_1} \mathrm{d}t \le \frac{1}{2}, \tag{44}$$

$$\beta(C_c) = \frac{1}{T\bar{C}}\int_{I_1} C(t)\,\mathrm{d}t, \tag{45}$$

where $\bar{C}$ is the average electricity price over the period of operation. As such, the revenue (42) is written more simply as

$$R(C_c) = T\bar{C}\cdot(1-2\alpha(C_c))^{1/2}\,(2\beta(C_c)-1)\,. \tag{46}$$

We note that both α and β are monotone decreasing functions of C_c, with $\alpha(C_0) = \beta(C_0) = 1$ and $\alpha(1) = \beta(1) = 0$. Furthermore, we require that $\alpha \ge 1/2$ to ensure that revenue (46) is a real-valued number. Hence, if we define C_{c0} as the price at which $\alpha(C_{c0}) = 1/2$, then we require that $C_c \ge C_{c0}$. The optimum value of C_c is therefore given by

$$C_c^* = \left\{ C_c \in [C_{c0}, 1] : \quad \frac{\partial R}{\partial C_c}(C_c^*) = 0 \right\}. \tag{47}$$

The functions $\alpha(C_c)$ and $\beta(C_c)$ (44) and (45) are well defined for any price function, allowing us to calculate the critical value of cost C_c at which switching occurs using (47). In general, this must be found numerically. For example, using the data from Fig. 4e ($C_0 = 0.3$, $T = 0.2$), we find $C_c = 0.710$ using (46) and (47), whereas the numerical solution switches at around $C_c \approx 0.711$ (and these values get closer as $T \to 0$).

The numerically calculated functions $\alpha(C_c)$, $\beta(C_c)$ and the revenue (46) are plotted for each of the different price functions in Fig. 6b–d for illustration. In each plot, the optimum value of the critical cost C_c occurs where the revenue is maximised, indicated with a marker. This constitutes a remarkably simple and operable solution for the optimal control since it only relies on manipulation of the price data $C(t)$ and does not require any heavy duty optimisation solver. The method can be applied to any price function $C(t)$ as long as the dimensionless period is small $T \ll 1$.

2.5 German electricity price data

Next we study the average German electricity price over the course of a week (2015–2021), which is the available data range that is freely available from [20]. In this case, the only free parameter is the period of operation T, since the value of $C_0 = 0.26$ is fixed.

Example optimal control strategies for short and long periods are shown in Fig. 7b, c. Meanwhile, the total revenue generated and the mean torque are plotted in Fig. 7a. As before, we see that for very short periods, a near-constant angular velocity is maintained, whereas for longer periods, ω fluctuates more strongly as the flywheel is accelerated before peaks in electricity price. All the results displayed here exhibit Bang-Bang (BB) behaviour only. For very long periods $T \gg 1$, Bang-Singular (BS) and purely Singular (S) behaviour is observed, but we do not display these results

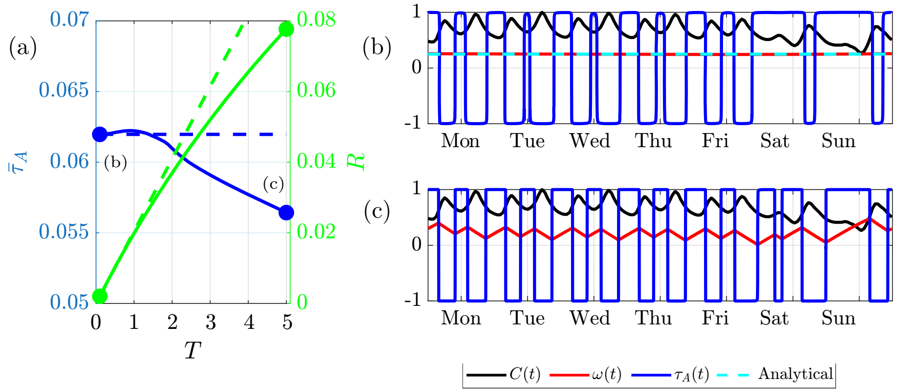

Fig. 7 Optimal control strategies for different values of T for the average German electricity price over the course of a week (2015–2021). Mean torque (left axis) and revenue (right axis) are plotted in **a** while example solutions are shown in **b**, **c**. Analytical approximations for small T are shown as dashed lines

here since they are not relevant for realistic parameter values (see later discussion in Sect. 4).

For very small periods $T \ll 1$ (which are more realistic), the near-constant angular velocity (e.g. see Fig. 7b) is $\omega \approx 0.25$, resulting in a mean torque of $\bar{\tau}_A \approx 0.063$. The critical cost C_c at which switching occurs is found by calculating α and β for this price function and finding the maximiser of revenue (46) and (47). This occurs at $C_c \approx 0.665$ (see Fig. 6c), whereas the numerically optimised solution switches at $C_c \approx 0.666$. This simple solution tells the flywheel operator to accelerate the device every time the price drops below 66% of the maximum price of the week, a protocol which is at the same time practical and optimal.

3 Operation with sails

In this section, we re-introduce the torque τ_S due to wind-driven sails attached to the upper surface of the flywheel. To begin with, we consider constant wind velocity and then extend the problem to account for variable wind. Throughout this section, we consider the sail torque τ_S as a modelled input, while we consider the applied torque τ_A as the control to be optimised.

We require a model for the torque τ_S generated by multiple sails mounted on the rotating structure in a crosswind. For a constant ambient windspeed, the aerodynamic torque at zero angular velocity is finite and positive; we denote this value by τ_W. As the rotational speed increases, the relative wind experienced by the sails decreases, and there exists a critical angular velocity ω_{crit} at which the net aerodynamic torque vanishes. This critical angular velocity corresponds to when the torque from each sail (due to lift and drag forces from the relative wind velocity) averages to a zero over an entire rotation. For angular velocities $\omega < \omega_{\text{crit}}$ the wind exerts a net accelerating torque, while for $\omega > \omega_{\text{crit}}$, the aerodynamic contribution becomes decelerating.

To capture these leading-order physical effects in a simple and analytically tractable manner, we assume that the sail-generated torque varies linearly with angular velocity according to

$$\tau_S(\omega(t)) = \tau_W \cdot \left(1 - \frac{\omega(t)}{\omega_{\text{crit}}}\right). \tag{48}$$

This expression enforces the physically motivated limits $\tau_S(0) = \tau_W$ and $\tau_S(\omega_{\text{crit}}) = 0$ and may be interpreted as a leading-order approximation to more detailed aerodynamic torque laws that depend on the relative wind speed. Both parameters, τ_W and ω_{crit} (see Appendix A for definitions), are treated as constants in the present analysis, which is equivalent to assuming a steady windspeed V_w.

Extensions to variable windspeed $V_w(t)$, together with practical estimates of τ_W and ω_{crit} under realistic offshore conditions, are described in Sects. 3.1 and 4. A more detailed examination of sail-generated torque for rotating structures in a crosswind is provided by [28], where the linear relationship (48) is shown to provide a good approximation under constant wind conditions. We verified that replacing the linear law (48) with a higher-order quadratic formulation does not qualitatively alter the optimal control structure of this study, nor the emergence of critical price switching. It is also noteworthy that an analogous linear dependence between torque and angular velocity appears in models of sprint cycling at fixed gear ratios [29, 30], where the cyclist's pedal plays a role analogous to a rotating sail.

Under the scalings (7), the dimensionless governing equation (including the sail torque) becomes

$$\frac{\mathrm{d}\omega}{\mathrm{d}t} = \tau_A(t) + \tau_{W0} - a\omega(t) - \omega(t)^2, \tag{49}$$

where $\tau_{W0} = \tau_W/\tau_{\max}$ and a is a dimensionless parameter defined by

$$a = \frac{\tau_W}{(I_D \tau_{\max})^{1/2}\, \omega_{\text{crit}}}. \tag{50}$$

Specifically, the dimensionless sail torque τ_S is given by the two new terms $\tau_{W0} - a\omega(t)$ in (49). As discussed later in Sect. 4, both τ_{W0} and a are estimated as order $\mathcal{O}(1)$ for realistic scenarios.

The Hamiltonian (see (17)) for the equivalent optimal control problem with sails is still linear in the control τ_A, as before. Hence, there may be intervals where τ_A is constant (such as bang-bang or bang-singular control). In the case where the applied torque is a constant $\tau_A = \tau_{A0}$, this has a steady-state angular velocity of

$$\omega = \left(\tau_{A0} + \tau_{W0} + \frac{a^2}{4}\right)^{1/2} - \frac{a}{2}, \tag{51}$$

which is nonnegative if $\tau_{A0} + \tau_{W0} \geq 0$ (i.e. if the total torque is positive when the device is stationary). In the case where $\tau_A(t)$ is not a constant, it can be substituted to rewrite the revenue as a functional of angular velocity, such that

$$R[\omega(t)] = \int_0^T -C(t)\left(\omega(t)\frac{\mathrm{d}\omega}{\mathrm{d}t} - \tau_{W0}\omega(t) + a\omega(t)^2 + \omega(t)^3\right)\mathrm{d}t. \tag{52}$$

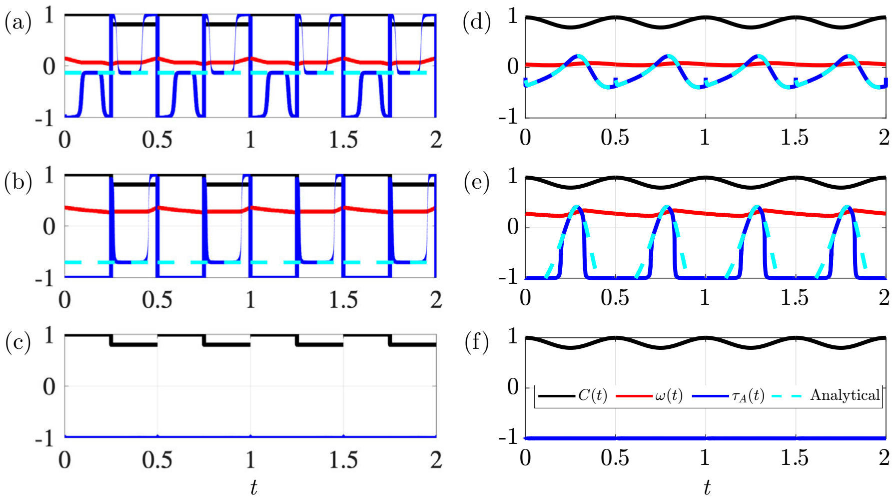

Fig. 8 Optimal control strategies in the presence of a constant windspeed in the case of **a**–**c** step-change price and **d**–**f** sinusoidal price. Parameter values are $C_0 = 0.8$, $T = 0.5$, $a = 2.0$, $\tau_{W0} = [0.2, 1, 5] \times a^2/3$ (from top to bottom). Dimensional parameter values are given in Appendix A, e.g. windspeed is taken as 10 m/s. Note, in **c**, **f**, the angular velocity is constant (56) ($\omega \approx 1.58$) but is not plotted since it lies above the upper axis limit

In this case, the Euler–Lagrange equation yields non-zero singular arcs of the form

$$\omega^*(t) = \frac{\dot{C} - 2aC + \sqrt{(2aC - \dot{C})^2 + 12\tau_{W0}C^2}}{6C}, \tag{53}$$

as well as stationary singular arcs $\omega^* = 0$. Due to the sails, it is now possible to generate revenue even when the electricity price is constant $C = 1$. For this case, (53) yields the constant-value singular arc

$$\omega^* = \frac{a}{3}\left(\sqrt{1 + 3\frac{\tau_{W0}}{a^2}} - 1\right), \tag{54}$$

which has corresponding negative applied torque

$$\tau_A^* = \frac{a^2}{9}\left(\sqrt{1 + 3\frac{\tau_{W0}}{a^2}} - 1 - 6\frac{\tau_{W0}}{a^2}\right) \leq 0, \tag{55}$$

indicating that revenue can be made even when the price is constant, in which case the flywheel acts like a regular wind turbine.

Numerical and analytical results are plotted in Fig. 8 in the case of a step-change and sinusoidal price curve. Results are plotted for different values of τ_{W0} and a to illustrate when drag from wind and water are imbalanced. Both singular and bang-bang behaviours are observed depending on the parameter values. For example, in Fig. 8a, b, the applied torque oscillates between its bounds and the constant singular value (55). In Fig. 8d, e, the applied torque is either zero or at its varying singular arc value (an analytical expression for this is found by inserting (53) into (49) but we do not include it here because it is long and complicated).

One interesting result occurs for $\tau_{W0} \gg a^2$ (i.e. wind drag much larger than water drag), where the applied torque simply remains at its maximum negative value $\tau_A = -1$ for all time, as shown in Fig. 8c, f. This is because the value of τ_A^* resulting from (53) lies outside the permitted bounds, such that $\tau_A^* < -1$. In this case, the system rotates at the steady state given by

$$\omega_0 = -\frac{a}{2} + \left(\tau_{W0} + \frac{a^2}{4} - 1\right)^{1/2}, \tag{56}$$

and a revenue $R = T\bar{C}\omega_0$ is generated purely by extracting energy from the wind, much like a regular wind turbine.

Another limit of interest is when the period is very short $T \ll 1$, as studied before. In this case, the angular velocity remains almost constant such that $\omega \approx \omega_0$, where

$$\omega_0 = -\frac{a}{2} + \left(\frac{a^2}{4} + \tau_{W0} + \bar{\tau}_A\right)^{1/2}. \tag{57}$$

We note that is now possible for the mean torque to be negative (unlike without sails), so long as $\bar{\tau}_A \geq -a^2/4 - \tau_{W0}$. We write the revenue (42) in terms of the functions α, β (44) and (45) using the fact that $\bar{\tau}_A = 1 - 2\alpha(C_c)$, such that

$$R = T\bar{C} \cdot \left(-\frac{a}{2} + \left[\frac{a^2}{4} + \tau_{W0} + 1 - 2\alpha(C_c)\right]^{1/2}\right)(2\beta(C_c) - 1). \tag{58}$$

The optimum value of C_c is therefore given by (47) where the minimum permitted value is defined by where $\alpha(C_{c0}) = 1/2(1 + a^2/4 + \tau_{W0})$. Hence, the presence of wind typically increases the critical cost above which the device should be charged, and results in more overall revenue. For example, in the case of the German electricity data, we find $C_c = 0.666$ without wind and $C_c = 0.569$ with wind using parameter values $a = 2$, $\tau_{W0} = 1$ (see discussion in Sect. 4).

3.1 Variable windspeed

In this next section, we will consider a wind-driven torque from the sails τ_S resulting from a non-constant windspeed $V_w(t)$. To adapt our model, we use (48) in combination with the fact that the dimensional values for τ_W and ω_{crit} are proportional to the windspeed according to $\tau_W \propto V_w^2$ and $\omega_{\text{crit}} \propto V_w$ (see (A12) and (A13) in Appendix A). Hence, by non-dimensionalising according to the scalings (7) (where the maximum windspeed over the period of operation $V_{\max}$ replaces the constant scaling for V_w), we arrive at the dimensionless governing equation

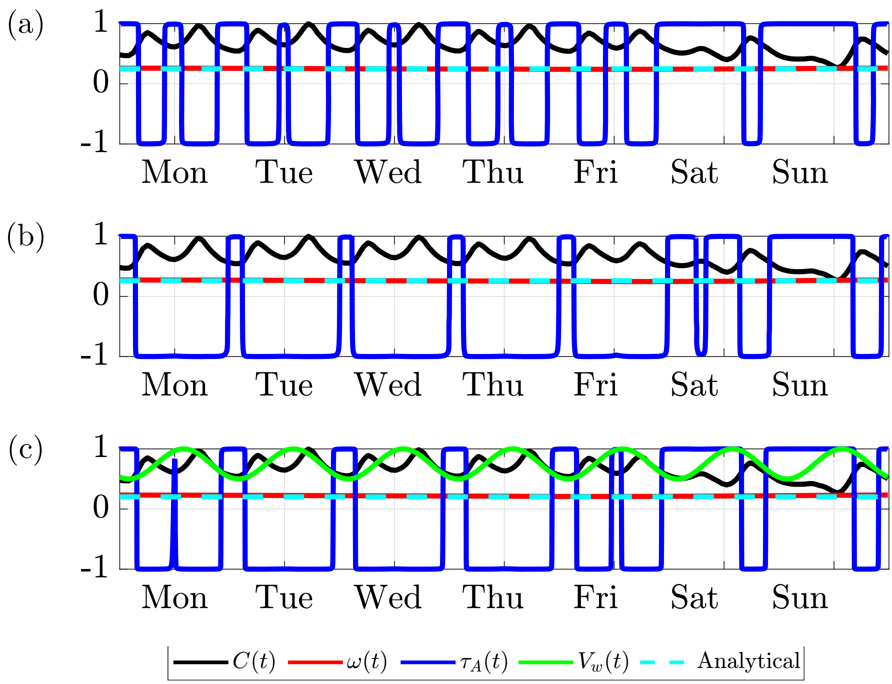

Fig. 9 Optimal control based on Germany's electricity price data (2015–2021). Dimensionless period is $T = 0.12$ in the case of **a** zero windspeed, $a = 0$, $\tau_{W0} = 0$, **b** constant windspeed, $a = 2$, $\tau_{W0} = 1$, and **c** variable windspeed (61) with $V_0 = 0.5$

$$\frac{\mathrm{d}\omega}{\mathrm{d}t} = \tau_A(t) + \tau_{W0} V_w(t)^2 - a V_w(t)\omega(t) - \omega(t)^2. \tag{59}$$

Hence, following the same steps as before, the singular angular velocity can be determined as

$$\omega^*(t) = \frac{\dot{C} - 2aCV_w + \sqrt{(2aCV_w - \dot{C})^2 + 12\tau_{W0}C^2V_w^2}}{6C}. \tag{60}$$

A simple demonstration of the effect of variable windspeed will be explored in the next section. For this, we use a periodic wind profile (for the sake of simplicity), which has its maximum in the afternoon at 2 pm and minimum at 2 am, such that

$$V_w = \frac{(1 + V_0)}{2} + \frac{(1 - V_0)}{2} \cos\left[\frac{2\pi}{24}(t_{\mathrm{hour}} + 10)\right], \tag{61}$$

where t_{hour} is the time given in hours and V_0 is the ratio of minimum to maximum windspeed.

4 Application to realistic scenarios

In this section, we discuss realistic parameter values for application scenarios. The parameters I and I_D are discussed in Appendix A. These measure the moment of inertia and the effective moment of inertia due to drag. Using parameter values in Table 1 for a 900 m radius flywheel, these are estimated as

$$I \sim 5.9 \times 10^{16}\ \mathrm{kg\,m^2}, \tag{62}$$

$$I_D \sim 2.6 \times 10^{11}\ \mathrm{kg\,m^2}. \tag{63}$$

In the Appendix, we also estimate the stationary torque τ_W due to wind at a constant speed of 10 m/s, such that

$$\tau_W \sim 5.24 \times 10^{8}\ \mathrm{kg\,m^2\,s^{-2}}. \tag{64}$$

For simplicity, we choose our torque constraint as $\tau_{\max} = \tau_W$, such that $\tau_{W0} = 1$. In other words, we assume that the maximum applied torque (due to engineering constraints) is the same as the maximum sail-driven torque available from a windspeed of 10 m/s. The dimensionless parameter a (A15) is estimated from the above values as $a = 2.0$. The dimensionless period of the oscillations is given by (13). Hence, taking $T_0 = 1$ week and using the above values, we find $T = 0.12$.

We apply the above parameter values to the optimal control problem corresponding to the German electricity price data taken from [20]. Results are plotted in Fig. 9a–c, in the case without wind, with constant windspeed and with variable windspeed (using (61) as our model for fluctuating windspeed with $V_0 = 0.5$). In all cases, the optimal angular velocity is nearly constant due to the small value of the dimensionless period $T = 0.12$, as discussed earlier. By taking the average of (59) over one period, we can approximate the near-constant value of the angular velocity as

$$\omega \approx \frac{1}{2}\left(-a\bar{V}_w + \sqrt{a^2\bar{V}_w^2 + 4\bar{\tau}_A + 4\tau_{W0}\bar{V}_w^2}\right), \tag{65}$$

where $\bar{\tau}_A$, $\bar{V}_w$ are the mean values of the applied torque and windspeed. The mean windspeed and applied torque are $\bar{V}_w = [0, 1, 0.75]$ and $\bar{\tau}_A = [0.0620, -0.4103, -0.2165]$ for the case without wind, with constant wind and with variable wind, respectively (note the negative mean values to exploit wind when present). This results in near-constant angular velocities (65) of $\omega = [0.2489, 0.2608, 0.2192]$, respectively. The approximation (65) is plotted as a dashed line in Fig. 9a–c, showing very close agreement with the numerics.

The critical cost C_c at which switching occurs can be found *a priori* by calculating $\alpha(C_c)$ and $\beta(C_c)$ (44) and (45) for this price function and finding the stationary point of (58). In the case of variable wind, the first bracketed term in (58) (representing the constant angular velocity) must be replaced with (65) to do this. Hence, the optimum switching price occurs at $C_c \approx [0.666, 0.569, 0.614]$ for the case without wind, with constant wind and with variable wind, respectively (showing very close comparison

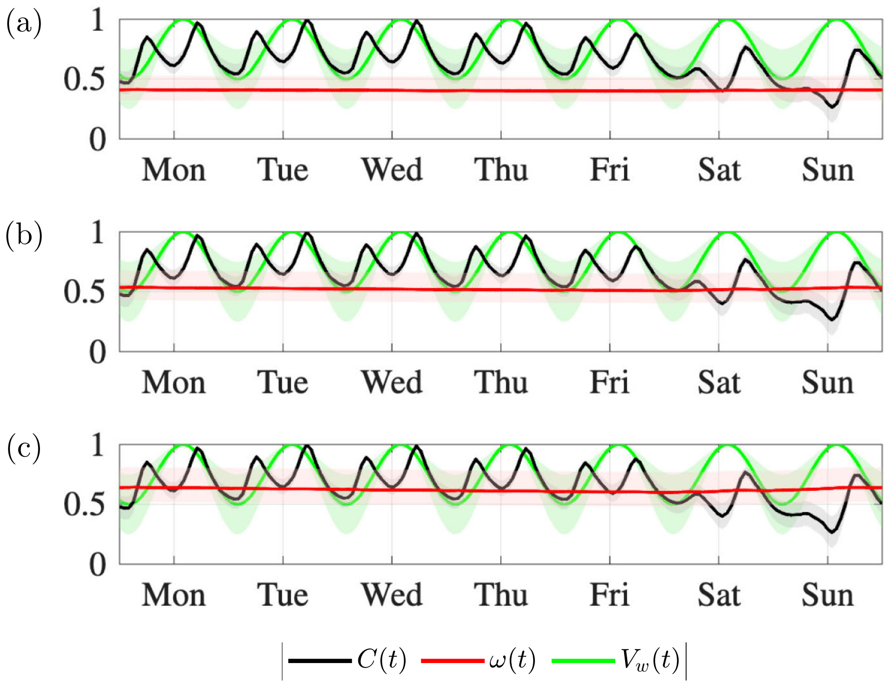

Fig. 10 Uncertainty analysis, using Germany's electricity price data (2015–2021) with variable wind (61) with parameters **a** $T = 0.049, a = 2.656, \tau_{W0} = 0.5$, **b** $T = 0.118, a = 2.029, \tau_{W0} = 1.0$ and **c** $T = 0.181, a = 1.704, \tau_{W0} = 1.5$. For each case, a range of price/wind profiles is given in the range $C_0 = 0.26 \pm 50\%$ and $V_0 = 0.5 \pm 50\%$

with numerically optimised solutions that switch at $C_c \approx [0.661, 0.572, 0.611]$). We also note that these predicted values of C_c can be inserted into the formula for mean torque $\bar{\tau}_A = 1 - 2\alpha(C_c)$, giving $\bar{\tau}_A = [0.0636, -0.4244, -0.2148]$, which are very close to the values quoted in the paragraph above. This indicates that our *a priori* prediction of the switching cost (based purely on the price data) is a robust method for predicting the optimal control behaviour—that is, without performing any numerical optimisation at all.

4.1 Uncertainty analysis

The dimensionless period T, which is defined in (13), plays a key role on the optimal control behaviour, and yet it depends on a number of parameters which are uncertain. In particular, the parameters I, I_D and $\tau_{\max}$ may vary significantly depending on the design of the flywheel system. In the following section, we explore how uncertainty in parameter values affects the optimal control behaviour (Fig. 10).

For the parameter $\tau_{\max}$, we estimate that engineering constraints may allow for $\pm 50\%$ deviations from the maximum sail-driven torque τ_W, i.e. $\tau_{\max} = 1 \pm 0.5$. To explore the uncertainty of the parameters I, I_D, we consider the range of parameter values listed in Table 1 (see Appendix A for more details). This results in a range of values

$$I \sim [2.16 - 12.82] \times 10^{16} \text{ kg m}^2, \tag{66}$$

$$I_D \sim [1.06 - 5.01] \times 10^{11} \text{ kg m}^2. \tag{67}$$

Hence, the dimensionless period is estimated in the range $T = 0.049 - 0.181$, with the shortest period $T = 0.049$ corresponding to $\tau_{\max} = 0.5$ and an associated value of the dimensionless wind parameter $a = 2.656$. Meanwhile the longest period $T = 0.181$ corresponds with $\tau_{\max} = 1.5$ and $a = 1.704$.

Meanwhile, the cost and wind profiles $C(t)$ and $V(t)$ may be subject to uncertainty. A simple way to explore this is by varying the minimum dimensionless values, C_0 and V_0. To do so, we explore a $\pm 50\%$ variation of each of these parameters, i.e. we assume $C_0 = 0.26 \pm 0.13$ and $V_0 = 0.5 \mp 0.25$. We have assumed that these uncertainties are inversely correlated for simplicity, i.e. a higher C_0 is paired with a lower V_0 to reflect the possible influence of an excess wind energy supply on the electricity market.

To demonstrate the results of our uncertainty analysis, we revisit Fig. 9c (i.e. German electricity data with variable windspeed) using the above ranges of possible parameter values. For all cases the period is relatively short, such that the optimal control is bang-bang around a critical price (as seen before), resulting in near-constant angular velocity throughout the week. Hence, despite the uncertainty in parameter values, the optimal methodology remains the same, i.e. switching about a critical price threshold is optimal.

In the case of lower, middle and upper range values of the period $T = [0.049, 0.118, 0.181]$, the near-constant optimal angular velocities are $\omega_0 \approx [0.406, 0.522, 0.621]$. Uncertainty due to wind and price conditions results in a range of velocities, as shown by the shaded regions in the figure (corresponding to $\pm$20–30% compared with original cost and wind conditions $C_0 = 0.26$, $V_0 = 0.5$). Corresponding values of the critical price are $C_c \approx [0.588, 0.553, 0.518]$ (for lower, middle and upper range values of the period), with 10–40% uncertainty due to the range of cost and wind conditions.

Our results demonstrate possible flywheel behaviours for a realistic range of values for each of the design parameters, as well as for a range of cost and wind profiles. For all realistic cases, bang-bang switching about a critical price is optimal, reflecting that our proposed control policy is highly robust in addition to being easy to implement.

5 Discussion

This study has explored how large floating flywheels could be operated as grid-scale energy storage devices in fluctuating electricity markets. By formulating and analysing an optimal control problem, we have identified both the range of possible control behaviours and the practical regimes that emerge under realistic parameter values.

A key result is that in realistic scenarios, the device operates in a simple regime where its angular velocity remains nearly constant, and the control policy reduces to switching between charging and discharging when the market price crosses a critical threshold. This is a strikingly practical outcome: it implies that complex forecasting and numerical optimisation are unnecessary. Instead, operation can be guided by a robust and easily implemented rule based solely on electricity price data.

The analysis also highlights the influence of hydrodynamic drag and the potential benefits of wind-driven sails. While drag losses are unavoidable, the addition of sails can offset these losses and even generate revenue when electricity prices are constant, effectively combining the functionality of a flywheel with aspects of a wind turbine. This suggests a pathway to improving the economic viability of floating flywheels, particularly in offshore environments where wind is available.

In terms of system-level implications, floating flywheels may offer several advantages relative to other storage technologies. Their large physical scale allows for GWh storage capacities, comparable to pumped hydropower but without the need for large mountains. Their offshore position also facilitates co-location with wind farms, reducing transmission constraints and enabling local balancing of supply and demand.

There are several limitations of our model and avenues for future work. Our model used simplified representations of hydrodynamic drag and wind torque; more detailed hydrodynamic and structural models will be required to predict precise performance. In a future study, it would be interesting to model the possible formation of a gyre at the centre of the flywheel, since this would reduce the drag at the inner walls and offer significant gains to the system (particularly since operation at constant angular velocity is typically optimal). Further, while this study assumed perfect knowledge of electricity prices, future work should incorporate uncertainty and stochastic control methods to account for the inherent unpredictability of markets [22, 23]. Coupling windspeed data with price forecasts may be particularly valuable in economies with high renewable dependance.

Overall, this work demonstrates that floating flywheels have the potential to contribute to future green energy systems by providing large-scale storage with simple and implementable control policies. The framework developed here provides both a theoretical foundation and a practical operational strategy, supporting the further development and potential deployment of this emerging technology.

Appendix A Approximate parameter scalings

Using the scaling for a cylindrical annulus, the moment of inertia is taken as

$$I \sim M R_s^2, \tag{A1}$$

where M is the total mass of the system, which is approximated as

$$M \sim \pi \rho_c H R_s^2, \tag{A2}$$

in terms of ρ_c, the density of the concrete that makes up the structure, R_s, the mean radius, and H, the total height. Inputting parameter values from Table 1 for a 900 m radius flywheel, we find

$$I \sim 5.9 \times 10^{16} \text{ kg m}^2. \tag{A3}$$

The parameter I_D requires a model for drag from the water. For the drag force between the wetted surface and the water, we use a quadratic inertial scaling (which is suitable for high Reynolds number flows)

$$F_D \sim \rho_w c_d A_w v^2, \tag{A4}$$

where ρ_w is the density of water, $A_w \sim 2\pi R_s H$ is the wetted surface area, c_d is an empirical drag coefficient, and $v \sim \omega R_s$ is the relative velocity between the fluid and the solid surface. As such, the drag-induced torque scales like

$$\tau_D \sim \rho_w c_d \pi \omega^2 R_s^3 H. \tag{A5}$$

Hence, the drag moment of inertia coefficient $I_D = \tau_D/\omega^2$ scales like

$$I_D \sim \rho_w c_d \pi R_s^3 H, \tag{A6}$$

where ρ_w is the density of water, and the drag coefficient c_d is approximated by the turbulent scaling [31]

$$c_d = \frac{0.075}{\log_{10} \mathrm{Re} - 2}. \tag{A7}$$

The Reynolds number Re is estimated as

$$\mathrm{Re} = \frac{\omega_r R_s^2}{\nu}, \tag{A8}$$

where $\nu = 10^{-6}$ m^2/s is the kinematic viscosity of water and ω_r is a representative value of the dimensional angular velocity, which we take as $\omega_r = 0.012$ rad/s (i.e. 1 rotation every 8.5 min). Hence, this gives us a Reynolds number of $\mathrm{Re} = 10^{10}$ and a corresponding drag coefficient of $c_d = 0.009375$. Hence, inputting parameter values from Table 1, we find

$$I_D \sim 2.6 \times 10^{11} \text{ kg m}^2. \tag{A9}$$

We can also estimate the stored kinetic energy of the flywheel as

$$E \sim \frac{1}{2} I \omega_r^2, \tag{A10}$$

resulting in an approximate stored energy of

$$E \sim 1.05 \,\text{GWh}. \tag{A11}$$

Finally, we need to approximate the torque due to the wind. The dimensional torque due to the wind (at zero angular velocity) scales like

$$\tau_W \sim \rho_a c_w N A R_s V_w^2, \tag{A12}$$

Table 1 Dimensional parameter values, motivated by discussions with *VerdErg Renewable Energy* (see [15])

Parameter (units)	Value	Uncertainty
R_s (m)	900	± 100
H (m)	12	± 5
ρ_a (kg m^{-3})	1.293	
ρ_c (kg m^{-3})	2400	
ρ_w (kg m^{-3})	1000	
A (m^2)	1000	± 500
V_w (m s^{-1})	10	± 10
ν (m^2/s)	10^{-6}	

where ρ_a is the density of air, N is the number of sails, c_w is an empirical dimensionless coefficient, A is the cross-sectional area of the sails, and V_w is the windspeed. The study of [28] suggests that $c_w \approx 3/8$ is a good approximations when N is large. For the purpose of this analysis, we shall take $N = 12$. In the same study [28], the critical angular velocity is calculated as

$$\omega_{\text{crit}} \approx \frac{2V_w}{R_s}. \tag{A13}$$

Hence, the corresponding dimensionless wind parameters τ_{W0} and a are given by

$$\tau_{W0} = \frac{\tau_W}{\tau_{\max}}, \tag{A14}$$

$$a = \frac{\tau_W R_s}{2V_w(\tau_{\max} I_D)^{1/2}}. \tag{A15}$$

As such, by inserting into (A12), the dimensional torque from the wind scales like

$$\tau_W \sim 5.24 \times 10^8 \,\text{kg}\,\text{m}^2\,\text{s}^{-2}, \tag{A16}$$

while the dimensional critical angular velocity scales like

$$\omega_{\text{crit}} \sim 0.022\,\text{rad/s}. \tag{A17}$$

For the sake of simplicity, we choose our torque constraint as $\tau_{\max} = \tau_W$, such that $\tau_{W0} = 1$. The dimensionless parameter a (A15) is estimated from the above values as $a = 2.0$.

Acknowledgements We would like to thank Peter Roberts, Robert Kettle and Lars Boerner from *VerdErg Renewable Energy* for financial support for this project and for many helpful discussions over the course of this research. Graham Benham thanks William Greenall for his insights on optimal control problems related to economic theory.

Author contributions R.W. and G.B. performed the numerical simulations, derived the analytical results, created the figures and wrote the main manuscript text. G.B. and I.H. supervised the project. All authors reviewed the manuscript.

Data availability An annotated Julia implementation of the optimal control framework developed in this study is publicly available to support reproducibility. The repository includes solver settings, discretisation details and example outputs. The code can be accessed at: https://github.com/gbenham/floating-flywheel-optimal-control.git

Declarations

Conflict of interest The authors declare no conflict of interest.

References

1. Suberu M, Mustafa M, Bashir N (2014) Energy storage systems for renewable energy power sector integration and mitigation of intermittency. Renew Sustain Energy Rev 35:499–514
2. Roberts L, Champneys A, Bell K, Bernardo M (2015) Analytical approximations of critical clearing time for parametric analysis of power system transient stability. IEEE J Emerg Sel Top Circuits Syst 5(3):465–476
3. Deutch J (2020) Is net zero carbon 2050 possible? Joule 4(11):2237–2240
4. National Energy System Operator: National Grid ESO: Future Energy Scenarios (FES). Technical report (2022)
5. Dehghani-Sanij AR, Tharumalingam E, Dusseault MB, Fraser R (2019) Study of energy storage systems and environmental challenges of batteries. Renew Sustain Energy Rev 104:192–208
6. Baines JA, Newman VG, Hanna IW, Douglas TH, Carlyle WJ, Jones IL, Eaton DM, Zeronian G (1983) Dinorwig pumped storage scheme. Part 1: design. Part 2: construction. Proc Inst Civ Eng 74(4):637–718
7. Yang Y, Bremner S, Menictas C, Kay M (2022) Modelling and optimal energy management for battery energy storage systems in renewable energy systems: a review. Renew Sustain Energy Rev 167:112671
8. Sim SB, Lee CH, Kim SK (2016) Study on the explosion and fire risks of lithium batteries due to high temperature and short circuit current. Fire Sci Eng 30(2):114–122
9. Kim SW, Park SG, Lee EJ (2022) Assessment of the explosion risk during lithium-ion battery fires. J Loss Prev Process Ind 80:104851
10. Costa CM, Barbosa JC, Gonçalves R, Castro H, Del Campo FJ, Lanceros-Méndez S (2021) Recycling and environmental issues of lithium-ion batteries: advances, challenges and opportunities. Energy Storage Mater 37:433–465
11. Budt M, Wolf D, Span R, Yan J (2016) A review on compressed air energy storage: basic principles, past milestones and recent developments. Appl Energy 170:250–268
12. Alva G, Lin Y, Fang G (2018) An overview of thermal energy storage systems. Energy 144:341–378
13. Sarbu I, Sebarchievici C (2018) A comprehensive review of thermal energy storage. Sustainability 10(1):191
14. Andersson J, Grönkvist S (2019) Large-scale storage of hydrogen. Int J Hydrogen Energy 44(23):11901–11919
15. VerdErg Renewable Energy (2022) GYRERG: wind energy storage on a Gigawatt-Scale. https://www.verderg.com/gyrerg. Accessed 12 Aug 2024
16. Díaz-González F, Sumper A, Gomis-Bellmunt O, Bianchi F (2013) Energy management of flywheel-based energy storage device for wind power smoothing. Appl Energy 110:207–219
17. Choudhury S (2021) Flywheel energy storage systems: a critical review on technologies, applications, and future prospects. Int Trans Electr Energy Syst 31(9):13024

18. Machlev R, Zargari N, Chowdhury N, Belikov J, Levron Y (2020) A review of optimal control methods for energy storage systems-energy trading, energy balancing and electric vehicles. J Energy Storage 32:101787
19. Wang L, Yu J, Chen Y (2011) Dynamic stability improvement of an integrated offshore wind and marine-current farm using a flywheel energy-storage system. IET Renew Power Gener 5(5):387–396
20. Ember-Energy. https://ember-energy.org/. Accessed 09 May 2025
21. Chiang A (2000) Elements of dynamic optimization. Waveland Press Inc, Long Grove
22. Bertsekas D (2012) Dynamic programming and optimal control: volume 1. Athena Scientific, Belmont
23. Riseth A (2018) Algorithms for decision making. PhD Thesis, University of Oxford. https://ora.ox.ac.uk/objects/uuid:a66e17dc-a626-4226-82f6-2d716f8690fd
24. Dunning I, Huchette J, Lubin M (2017) JuMP: a modeling language for mathematical optimization. SIAM Rev 59(2):295–320
25. Wächter A, Biegler L (2006) On the implementation of an interior-point filter line-search algorithm for large-scale nonlinear programming. Math Program 106:25–57
26. Cirocco L, Belusko M, Bruno F, Boland J, Pudney P (2016) Maximising revenue via optimal control of a concentrating solar thermal power plant with limited storage capacity. IET Renew Power Gener 10(5):729–734
27. Pitcher AB (2009) Mathematical modelling and optimal control of constrained systems. PhD Thesis, University of Oxford. https://ora.ox.ac.uk/objects/uuid:044a26ab-99dc-4b34-b4a3-04e5c0d61ba0
28. Ward R, Benham G, Hewitt I (2025) Optimal sail angles to drive circular motion.(submitted)
29. Dorel S, Hautier C, Rambaud O, Rouffet D, Van Praagh E, Lacour J, Bourdin M (2005) Torque and power-velocity relationships in cycling: relevance to track sprint performance in world-class cyclists. Int J Sports Med 26(09):739–746
30. Benham G, Cohen C, Brunet E, Clanet C (2020) Brachistochrone on a velodrome. Proc R Soc A 476(2238):20200153
31. Hadler J (1958) Coefficients for international towing tank conference 1957 model-ship correlation line. Technical report